Biophysical Journal, Volume *110*

Supplemental Information

Cellular Contraction and Polarization Drive Collective Cellular Motion

Jacob Notbohm, Shiladitya Banerjee, Kazage J.C. Utuje, Bomi Gweon, Hwanseok Jang, Yongdoo Park, Jennifer Shin, James P. Butler, Jeffrey J. Fredberg, and M. Cristina Marchetti

Monolayer stress microscopy

Here we detail our experimental technique for recovering intercellular stresses from tractions, called monolayer stress microscopy (MSM; Refs. 8, 23). The concept underlying monolayer stress microscopy is force equilibrium applied to the cell layer. Assuming the layer to be thin with no variation through the thickness, the two equilibrium equations are

$$\begin{aligned} \frac{\partial \sigma_{xx}}{\partial x} + \frac{\partial \sigma_{xy}}{\partial y} + \frac{T_x}{h} &= 0 \\ \frac{\partial \sigma_{xy}}{\partial x} + \frac{\partial \sigma_{yy}}{\partial y} + \frac{T_y}{h} &= 0, \end{aligned} \tag{1}$$

where σ_{ij} are components of the in-plane stress tensor, T_i is the i-th component of the traction vector applied by the substrate to the monolayer, and h is the thickness of the monolayer. These equations are independent of the constitutive properties of the monolayer; they result directly from a balance of forces. Note that in one dimension (chosen in the x direction) Eqs. (1) would reduce to the single equation

$$\frac{\partial \sigma_{xx}}{\partial x} + \frac{T_x}{h} = 0\,, \tag{2}$$

which can immediately be integrated to obtain the cellular stress σ_{xx} with no assumption on the form of the constitutive equation.

In two dimensions, however, the stress tensor has three unique components, so a third equation is required. In the original implementation of MSM (8, 23), the monolayer was assumed to behave as a linear elastic material, giving the following two-dimensional (2D) constitutive relationship between stress and strain:

$$\sigma_{ij} = \frac{E\nu}{1-\nu^2}\varepsilon_{kk}\delta_{ij} + \frac{E}{1+\nu}\varepsilon_{ij}, \tag{3}$$

where E is Young's modulus, ν is Poisson's ratio, and ε_{ij} are components of the in-plane strain tensor. Here summation over repeated indices is implied. Assuming the monolayer is homogeneous, the constitutive equation combined with Eqs. 1 and compatibility of strain (requiring that the strain be the derivative of a unique vector field),

$$\frac{\partial^2 \varepsilon_{xx}}{\partial y^2} + \frac{\partial^2 \varepsilon_{yy}}{\partial x^2} = 2\frac{\partial^2 \varepsilon_{xy}}{\partial x \partial y}, \tag{4}$$

give the Beltrami–Michell equation (23),

$$\nabla^2 (\sigma_{xx} + \sigma_{yy}) = -\frac{1+\nu}{h}\left(\frac{\partial T_x}{\partial x} + \frac{\partial T_y}{\partial y}\right). \tag{5}$$

Together, Eqs. 1 and 5 can be solved for the three independent components of the stress tensor σ_{ij}. Note that the equations are independent of Young's modulus; furthermore it has been shown that dependence on Poisson's ratio is sufficiently weak to make it negligible (23).

We now discuss the case where the cell layer is a linear viscous material. In this case the 2D constitutive equation is

$$\sigma_{ij} = -p\delta_{ij} + (\mu_b - \mu_s)\,\dot{\varepsilon}_{kk}\delta_{ij} + 2\mu_s\dot{\varepsilon}_{ij}, \tag{6}$$

where p is the thermodynamic pressure, μ_b and μ_s are the bulk and shear viscosities, respectively, and the overdot represents a partial derivative in time. Requiring that the strain rate $\dot{\varepsilon}_{ij}$ be the derivative of a unique vector field (the local velocity) yields a compatibility equation

$$\frac{\partial^2 \dot{\varepsilon}_{xx}}{\partial y^2} + \frac{\partial^2 \dot{\varepsilon}_{yy}}{\partial x^2} = 2\frac{\partial^2 \dot{\varepsilon}_{xy}}{\partial x \partial y}. \tag{7}$$

If we assume the layer to be incompressible and neglect pressure gradients, we can combine Eqs. 1, 6, and 7 to obtain

$$\nabla^2 (\sigma_{xx} + \sigma_{yy}) = -\frac{\left(\frac{2\mu_b}{\mu_b+\mu_s}\right)}{h} \left(\frac{\partial T_x}{\partial x} + \frac{\partial T_y}{\partial y}\right), \tag{8}$$

which is equivalent to Eq. 5. In this case the conventional method used to infer stress from traction in MSM applies regardless of whether a material is elastic or viscous. In general, however, in a fluid density fluctuations are not slaved to strain fluctuations and an additional condition is needed to determine the pressure. Whether such a pressure exists in a cell monolayer remains unknown.

Recent work by Zimmermann et al. (17) has provided independent validation of the method used in MSM. In their verification, Zimmermann et al. simulated collective cell motion using a particle-based model. The particles in the model represented cells, and were able to flow freely past one another with no memory of their previous position, therefore behaving like a fluid where particles do not maintain the same neighbors in the course of time. Zimmermann et al. then computed the stresses directly from the simulations and compared them to stresses computed with MSM. The comparison showed close agreement (17), suggesting that MSM can be applied to either an elastic or a viscous material, and that pressure variations do not play an important role in the viscous case.

Minimal physical model of collective cell motion

Continuum model. Here we provide a detailed description of the minimal physical model introduced in the main text. We consider a thin film of cell monolayer confined to a circular micro-pattern of radius R with average height h. We describe the monolayer as an elastic continuum whose vector displacement at position $\mathbf{r}$ and at time t is given by $\mathbf{u}(\mathbf{r},t)$. The local displacements of the monolayer are coupled to two internal degrees of freedom, the concentration $c(\mathbf{r},t)$ of a regulatory chemical controlling cell contractility, and a dimensionless vector field $\mathbf{p}(\mathbf{r},t)$ controlling the angle of misalignment between local cell motion and propulsive traction forces. The magnitude of $\mathbf{p}$ accounts for the amount of misalignment between cell motion and traction, whereas its orientation defines the direction of the thrust force acting on the cell. In the absence of external forces, in-plane force balance gives,

$$\partial_j \Sigma_{ij} + \partial_z \Sigma_{iz} = 0\,, \tag{9}$$

where Σ is the stress tensor of the monolayer and latin indices denote in-plane coordinates x and y. For $h \ll R$, we average the force balance across the z-direction, assuming that the top surface of the monolayer at $z = h$ is stress free, i.e. $\Sigma_{iz}|_{z=h} = 0$. This gives us,

$$h\partial_j \sigma_{ij} = \Sigma_{iz}|_{z=0}, \tag{10}$$

where $\sigma_{ij}(x,y) = h^{-1}\int_0^h dz\, \Sigma_{ij}(x,y,z)$ is the thickness averaged stress tensor of the monolayer equivalent to what is measured in experiments. We identify the shear stress at the cell–substrate interface, $\Sigma_{iz}|_{z=h}$, as the traction stress T_i exerted by the cell on the substrate. This gives us the following relation between monolayer stress and traction,

$$T_i = h\partial_j \sigma_{ij}, \tag{11}$$

The monolayer stress tensor is given by the sum of passive elastic and active elements connected in parallel (Fig. 3b), $\sigma_{ij} = \sigma^{\mathrm{el}}_{ij} + \sigma^{\mathrm{a}}_{ij}$, where the passive elastic component of the stress tensor, $\sigma^{\mathrm{el}}_{ij}$, is assumed to be isotropic and homogeneous. It is given by,

$$\sigma^{\mathrm{el}}_{ij} = B\varepsilon_{kk}\delta_{ij} + 2G\left(\varepsilon_{ij} - \frac{1}{2}\delta_{ij}\varepsilon_{kk}\right)\,. \tag{12}$$

B and G are respectively the in-plane bulk and shear elastic moduli of the monolayer, ε_{ij} the symmetrized strain tensor, $\varepsilon_{ij} = \frac{1}{2}(\partial_i u_j + \partial_j u_i)$ and δ_{ij} the Kronecker delta. The active stress σ^{a}_{ij} is taken to be proportional to the logarithm of the concentration field, $\log(c/c_0)$, where c_0 is the concentration at chemical equilibrium when no stress is generated. Although we are not aware of any direct measurement of active stress in live cells and their relationships with myosin concentration and chemical potential of ATP, the logarithmic dependence of active stress on concentration follows from two simple assumptions. First, we assume the presence of weak to moderate activity level in cells such that the stress depends linearly on the chemical potential. Second, the chemical potential difference is related logarithmically the concentration of reactants and products given the partial pressure of the molecules are linearly dependent on the concentration. We thus have,

$$\sigma^{\mathrm{a}}_{ij} = \beta \log(c/c_0)\delta_{ij} \,, \tag{13}$$

where $\beta > 0$ is the magnitude of the active contractile stresses generated by molecular motors and c_0 is the equilibrium concentration. The assumption of isotropic stress is consistent with the stress field measured in our experiments using monolayer stress microscopy. Our principal stress analysis reveals that the stress ellipses in the monolayer typically have low aspect ratio with a quotient of maximum shear to tension less than 0.2 (Supporting Fig. S9). The dynamics of the displacement field, $\mathbf{u}(\mathbf{r},t)$, is given by

$$\zeta \partial_t u_i = f p_i + h \partial_j \sigma_{ij} \tag{14}$$

where ζ describes viscous friction with the substrate and the constant f is the magnitude of the coupling between polarization and motion and quantifies the strength of the propulsion force. The resultant traction applied by the cells on the substrate is thus, $\mathbf{T} = \zeta \partial_t \mathbf{u} - f\mathbf{p}$. The dynamics of the concentration field $c(\mathbf{r},t)$ is given by,

$$\partial_t c + \boldsymbol{\nabla} \cdot (c \partial_t \mathbf{u}) = -\frac{1}{\tau}(c - c_0) + \alpha c_0 \varepsilon_{kk} \,, \tag{15}$$

where τ is the timescale of actomyosin relaxation to equilibrium and α is the rate of production of c due to cellular stretching. The second term on the left hand side of Eq. (15) describes convection of chemicals by local cell motion. The dynamics of the polarization field $\mathbf{p}(\mathbf{r},t)$ is given by,

$$\partial_t p_i = a\left(1 - |\mathbf{p}|^2\right) p_i + \kappa \nabla^2 p_i + w \partial_i (c/c_0) \,, \tag{16}$$

where the first two terms allow for the onset of a homogeneously polarized system, $|\mathbf{p}| = 1$, and a (> 0) is the rate of relaxation to the homegeneous state $|\mathbf{p}| = 1$. Local cost of fluctuations in polarization is characterized by an isotropic stiffness κ with dimensions of diffusivity; it describes the tendency of cell polarization to align with its neighbors. The active coupling w describes the local rate of alignment of cell polarization with the gradients of the concentration field.

Numerical solution in circular geometry. We numerically solve the model equations in a circular geometry by assuming in-plane rotational symmetry such that all quantities depend solely on the radial coordinate, r. Rotational symmetry in polar coordinates implies that shear stresses $\sigma_{r\theta}$ vanish and the dynamics of the radial displacement field are solely governed by normal stresses, in agreement with the experiments (Supporting Fig. S9). The equation of motion for radial displacements u_r is given by,

$$\zeta \partial_t u_r = f p_r + h\left(\partial_r \sigma_{rr} + \frac{1}{r}(\sigma_{rr} - \sigma_{\theta\theta})\right) \,, \tag{17}$$

where σ_{rr} and $\sigma_{\theta\theta}$ define the radial and orthoradial components of the normal stress in the monolayer, given by,

$$\sigma_{rr} = B\left(\partial_r u_r + \frac{u_r}{r}\right) + G\left(\partial_r u_r - \frac{u_r}{r}\right) + \beta \log(c/c_0) \,, \tag{18}$$

$$\sigma_{\theta\theta} = B\left(\partial_r u_r + \frac{u_r}{r}\right) - G\left(\partial_r u_r - \frac{u_r}{r}\right) + \beta \log(c/c_0) \,. \tag{19}$$

The equation governing the dynamics of c is given by,

$$\partial_t c + \frac{1}{r}\partial_r\left(rc\partial_t u_r\right) = -\frac{1}{\tau}\left(c - c_0\right) + \alpha c_0\left(\partial_r u_r + \frac{u_r}{r}\right) \,. \tag{20}$$

Finally, the equation governing the dynamics of radial polarization, p_r, is given by

$$\partial_t p_r = a\left(1 - p_r^2\right) p_r + \frac{\kappa}{r}\partial_r(r\partial_r p_r) + w\partial_r(c/c_0) \,. \tag{21}$$

The homogeneous solutions to the above equation, $p_r = \pm 1$, describe uniformly polarized states of the cell monolayer with the cell motion pointing radially outwards for $p_r = 1$ and inward for $p_r = -1$. The solution $p_r = 1$ describes the tendency of cell motion to polarize towards the free space at the exterior of the cell island, consistent with *kenotaxis* (10).

To solve the above equations, we assume that no external forces act at the outer boundary such that $\sigma_{ij} n_j = 0$ where n_j is the outward unit normal vector to the boundary. This translates to the boundary condition $\sigma_{rr}(R) = 0$ in circular geometry. We model adhesion with the micropattern by anchoring a hookean spring of stiffness 0.03 Pa/μm at the boundary of the cell monolayer. We choose a no-flux boundary condition for c and p_r, such that $\partial_r c(R) = 0$, and the gradients of the polarization variable at the outer boundary is zero, $\partial_r p_r(R) = 0$. We also assume that the monolayer is initially undeformed, $u(r,0) = 0$, and unpolarized, $p_r(r,0) = 0$, with an equilibrium concentration of contractile elements, $c(r,0) = c_0$. We then integrate numerically Eqs. (17), (20) and (21) with the given initial and boundary conditions by means of the Runge–Kutta–Fehlberg method. We solve three different implementations of the model:

- **u**-**p** *model.* Radial displacement u_r is coupled only to p_r and the concentration field is assumed to be constant, $c = c_0$. In this case no wave-like behavior is obtained (Supporting Fig. S6 d–f), indicating that the mechanochemical coupling between c and u_r is crucial to reproduce the waves of oscillatory motion.

- **u**-*c* *model.* Displacement u_r is coupled to c only. The polarization field and hence the propulsion force fp_r are set to zero. In this case we obtain standing waves qualitatively similar to those seen in experiments (Supporting Fig. S6 a–c). However, the traction is proportional to velocity, in contrast to the misalignment observed in experiments.

- **u**-*c*-**p** *model*. Here we use the full equations of motion, coupling u_r to both c and p_r and are able to quanitatively reproduce the experimental trends (Fig. 3).

Finite difference spatial discretization scheme. To solve Eqs. (17), (20) and (21) numerically, we first spatially discretize the equations using the central finite difference method and then integrate them numerically by means of the Runge–Kutta–Fehlberg method. At every time step, the spatial domain spans from 0 to

R, where R is the radius of the cell monolayer. The numerical approximation to the functions $u_r(r,t)$, $c(r,t)$ and $p_r(r,t)$ at the spatial grid point $r_i = i\Delta r$ with $\Delta r = R/(N-1)$ and $i = 1, N-2$, are denoted as $u_n^i(t_n)$, $c_n^i(t_n)$ and $p_n^i(t_n)$ respectively. In the following, we drop the argument t_n of the functions for convenience. Substituting Eqs. (18) and (19) in Eq. (17), the equation of motion is spatially discretized as follows,

$$\zeta \partial_t u_n^i = f p_n^i + h\left[(B+G)\left(\left(\frac{u_n^{i+1}+u_n^{i-1}-2u_n^i}{\Delta r^2}\right)+\left(\frac{u_n^{i+1}-u_n^{i-1}}{2r_i\Delta r}\right)-\frac{u_n^i}{r_i^2}\right)+\beta\left(\frac{c_n^{i+1}-c_n^{i-1}}{2c_n^i\Delta r}\right)\right]. \quad (22)$$

The spatial discretization of Eq. (20) gives,

$$\partial_t c_n^i + \frac{1}{r_i}\left(c_n^i \partial_t u_n^i\right) + \left(\frac{c_n^{i+1}-c_n^{i-1}}{2\Delta r}\right)\partial_t u_n^i + c_n^i\left(\frac{\partial_t u_n^{i+1}-\partial_t u_n^{i-1}}{2\Delta r}\right) = -\frac{1}{\tau}\left(c_n^i - c_0\right) + \alpha c_0\left(\frac{u_n^{i+1}-u_n^{i-1}}{2\Delta r}+\frac{u_n^i}{r_i}\right). \quad (23)$$

The spatial discretization of Eq. (21) gives,

$$\partial_t p_n^i = a\left(1-(p_n^i)^2\right)p_n^i + \kappa\left(\frac{p_n^{i+1}+p_n^{i-1}-2p_n^i}{\Delta r^2}\right)+\kappa\left(\frac{p_n^{i+1}-p_n^{i-1}}{2r_i\Delta r}\right)+w\left(\frac{c_n^{i+1}-c_n^{i-1}}{2c_0\Delta r}\right). \quad (24)$$

At $i = 0$, the boundary conditions for the above discretized equations are given by: $\zeta\partial_t u_n^0 = 0$, $\partial_t c_n^0 = -\frac{1}{\tau}\left(c_n^0 - c_0\right)$ and $\partial_t p_n^0 = a\left(1-(p_n^0)^2\right)p_n^0 + 2\kappa\left(\frac{p_n^1 - p_n^0}{\Delta r^2}\right)$. Here we applied the same boundary conditions, $\partial_r c(0) = \partial_r p_r(0) = 0$ and l'Hospital's Rule to resolve the singularity at $i = 0$. At $i = N-1$, the boundary condition $\sigma_{rr}(R) = 0$ gives the value of the ghost point $u_n^N = u_n^{N-2} - \frac{2\Delta r}{B+G}\left[(B-G)\left(\frac{u_n^{N-1}}{R}\right)+\beta\log\left(\frac{(c_n^{N-1})}{c_0}\right)\right]$ in Eqs. (22) and (23). The boundary condition $\partial_r c(R) = 0$ gives the value of the ghost point $c_n^N = c_n^{N-2}$ in Eqs. (22), (23) and (24) while the boundary condition $\partial_r p_r(R) = 0$ gives the value of the ghost point $p_n^N = p_n^{N-2}$ in Eq. (24). Eqs. (22), (23) and (24) are then integrated numerically with the given initial and boundary conditions, using the Runge–Kutta–Fehlberg method.

Model parameters. While the model parameters are cell-type dependent, they are chosen so as to quantitatively reproduce our experimental data on MDCK cell monolayers for traction, velocity and intercellular stress. Specifically, the radius of the cell monolayer is taken to be $R = 350\ \mu$m and the values of the elastic moduli, B and G, and the contractile stress β are taken to be of the same order of magnitude with the experimentally measured effective elastic modulus K of the monolayer. The values of the timescales regulating the chemical dynamics, τ and α^{-1}, are tuned so as reproduce the experimentally measured time period of oscillations $\sim$6 hrs. The remaining values are chosen within the order of magnitudes reported in prior literature. A complete list of the parameter values is given in Supporting Table S1.

Experimental validation of the model predictions.

- *Contractile activity generates effective elasticity and mechanical waves.* Our model predicts that the coupling between contractility and the monolayer strain yields an effective bulk modulus, $K = B + \alpha\tau(\beta + fw/2ah)$ that is greater than the passive bulk elastic modulus of the material (13). Furthermore, in our model waves arise due to a local feedback between rate of production of c and mechanical strain in the monolayer. This is consistent with our experimental data which shows that the treatment with blebbistatin (an inhibitor of myosin-based contractility) reduces the effective elastic modulus K of the cell monolayer by an order of magnitude and eliminates the waves (Fig. 4 a–d).

Supporting Table S1: Model parameters.

Parameter	Physical Meaning	Numerical Value
ζ	Viscous friction with the substrate	0.2 Pa hr/μm
f	Propulsion force	10 Pa
R	Monolayer radius	350 μm
h	Monolayer thickness	3 μm
B	Bulk elastic modulus	300 Pa
G	Shear elastic modulus	200 Pa
β	Magnitude of the active stress	600 Pa
τ	Timescale of relaxation of c	1.17 hrs
α	Rate of production of c due to cell stretching	2.14 hr^{-1}
a	Rate of relaxation to a homogeneously polar state	0.78 hr^{-1}
κ	Stiffness constant characterizing the cost of local changes in $\mathbf{p}$	8.75 μm^2/min
w	Controls the rate of alignment of $\mathbf{p}$ with the gradients of c	2.08 μm/min

- *Cell polarization aligns with the gradients of contractile tension*. Our minimal model incorporates feedback between $\mathbf{p}$ and c such that $\partial_t \mathbf{p} \propto \nabla(c/c_0)$. Because the active stress σ_a goes as $\log(c/c_0)$, we expect that $\partial_t \mathbf{p} \propto \nabla\sigma$. Furthermore, since $\mathbf{T} = \zeta\mathbf{v} - f\mathbf{p}$, and $\mathbf{v}$ averages to 0 over one period of oscillation, we expect that $\langle \partial(-\mathbf{T})/\partial t \rangle \sim \langle \nabla\sigma \rangle$, where the angular brackets denote time average over one period of oscillations. When we compare directions of $\langle \partial(-\mathbf{T})/\partial t \rangle$ and $\langle \nabla\sigma \rangle$, we find alignment (Supporting Fig. S10).

- *Cell polarization exists even in the absence of contractility*. Our experimental data show that after treatment with blebbistatin, the traction and the velocity field of the monolayer are misaligned on average, with the traction vectors pointing radially inward at the perimeter of the island and cell motion polarized radially outwards (Supporting Fig. S11). This behavior of cells to polarize their motion radially outward is consistent with the results of the *u–p model* that reproduces the anti-alignment between traction and velocity in the absence of contractility (Supporting Fig. S6 d,e).

- *Scaling of the time period with monolayer size*. A linear stability analysis of our continuum model predicts a characteristic frequency of oscillatory waves in the monolayer given by (13),

$$\omega_0(q) \simeq q\sqrt{hK/\tau\zeta}\,, \tag{25}$$

where q is the radial wave vector. At length scales comparable to the monolayer size, $q \simeq 1/R$, we get the following analytical expression for the time period,

$$T \simeq 2\pi R\sqrt{\tau\zeta/hK}\,. \tag{26}$$

Our model thus predicts a linear scaling relation between the time period of oscillations and the monolayer radius, in agreement with experimental measurements (7).

Supporting Figures

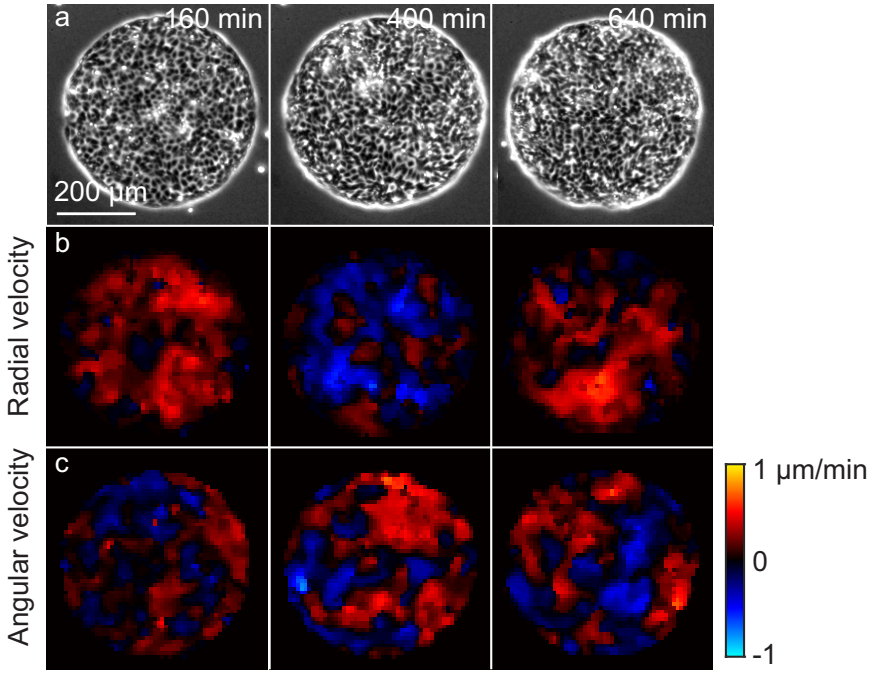

Supporting Figure S1: Full velocity field of the the monolayer shown in Fig. 1. (a) Phase contrast images at three different time points. (b, c) Radial (b) and angular (c) components of the cellular velocity.

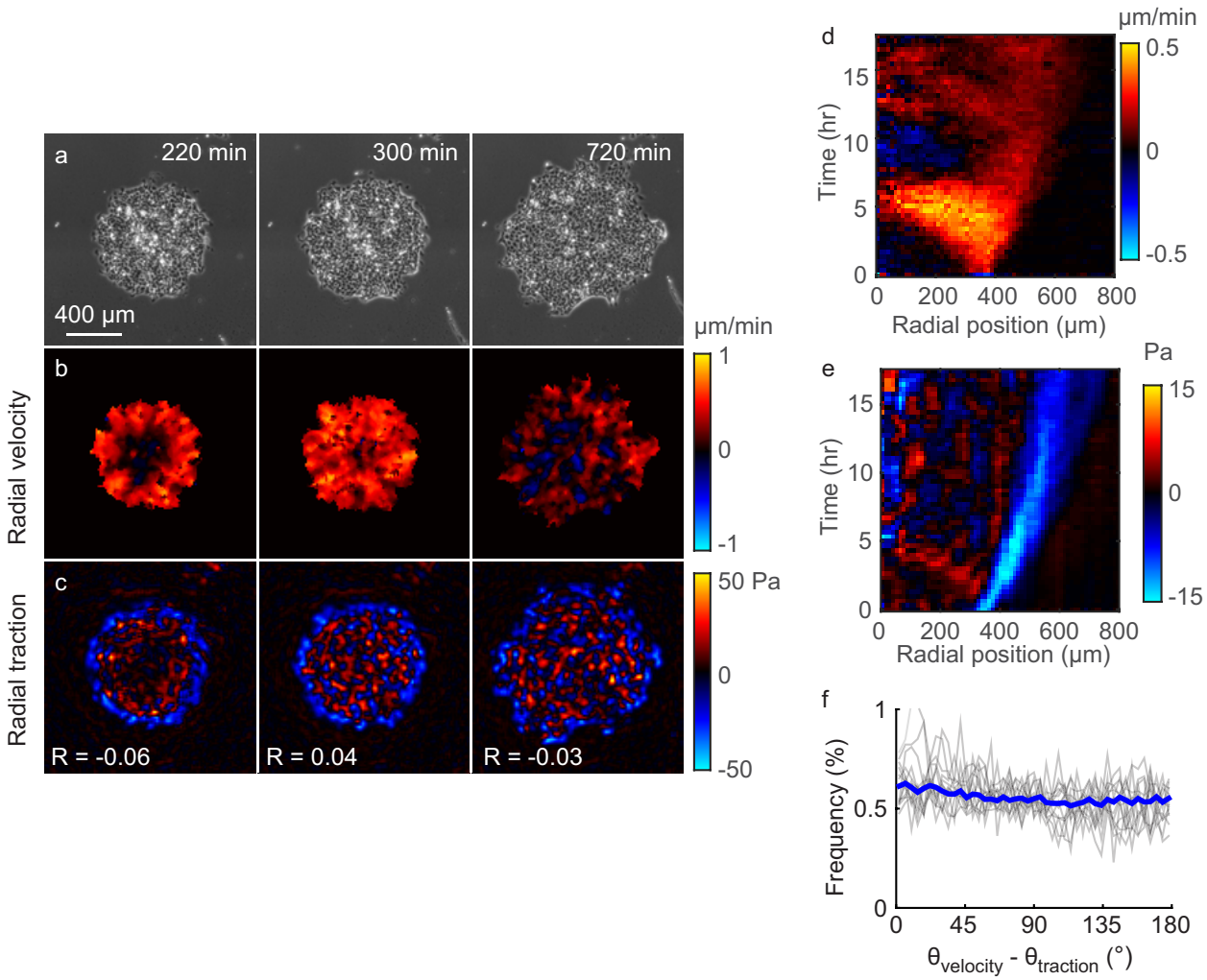

Supporting Figure S2: In expanding cellular monolayers, cellular tractions align in a different direction than cellular velocities. (a) MDCK cells are micropatterned into 700 μm islands using a PDMS mask on a polyacrylamide gel. When the mask is removed, the cells migrate outward. Times are in minutes after removing the mask. (b) Cell velocities are measured using particle image velocimetry, and the radial component of the velocity vector is plotted. The positive direction (red) represents outward motion. At early times (220 min), cells at the periphery move outward; later (300 min), all cells move outward. Once the island is fully spread (720 min), cells move either inward or outward. (c) Radial component of traction applied by the cells to the substrate. Areas in blue indicate regions where the cells pull inward on the substrate; this inward force, if unbalanced, would accelerate the cells outward. The relationship between velocity and traction is evaluated with Pearson's correlation coefficient, R. (d, e) Kymographs of radial velocity (d) and radial traction (e). At all points in time, neither the spatial map of tractions (c) nor the averaged tractions (e) correlate with the velocity. (f) Histogram of the angle between the velocity and traction vectors. Each gray line shows a single point in time for the cell island; the blue line shows all points in time.

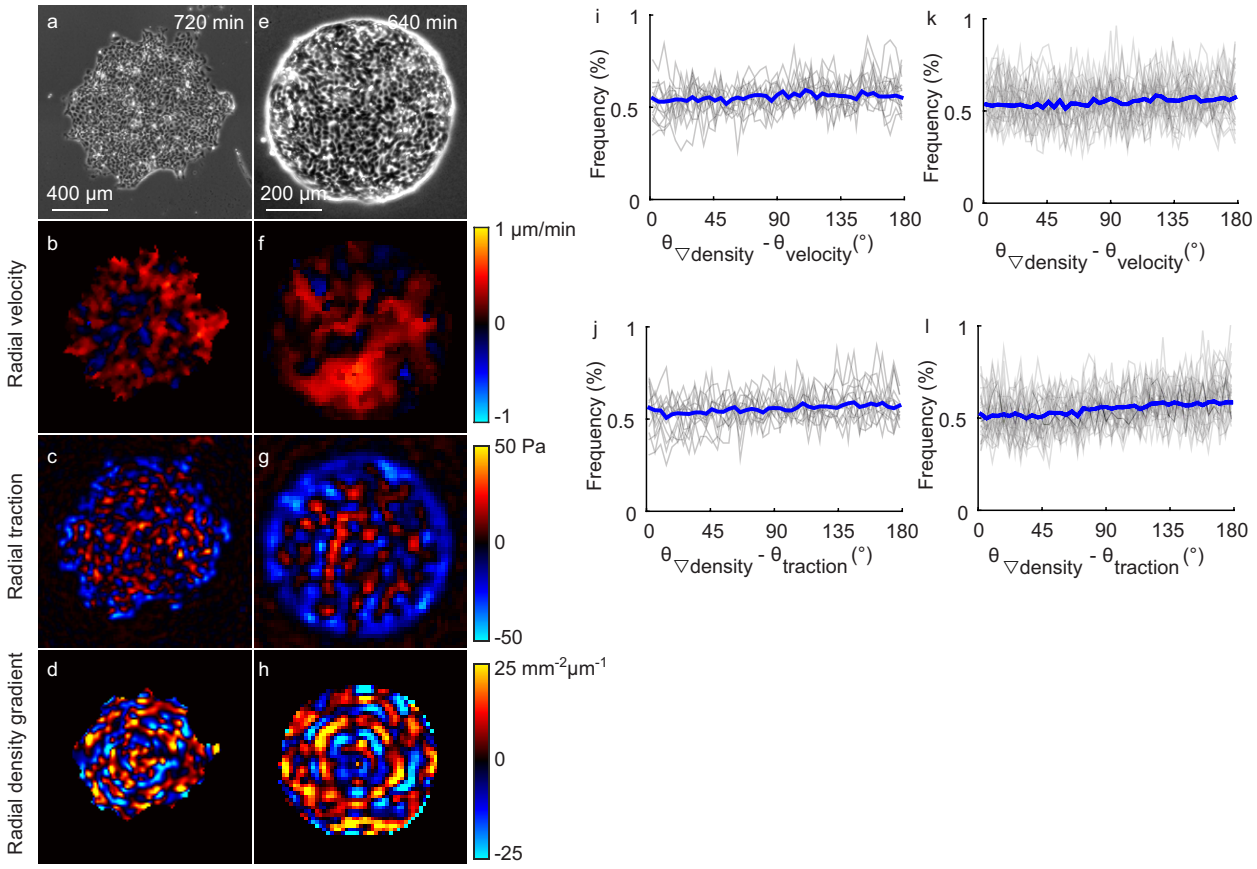

Supporting Figure S3: Gradients in local number density do not drive collective motion in expanding or confined monolayers. (a) Phase contrast image of MDCK cells in an expanding island 720 min after removing the mask. (b–d) The radial components of velocity (b) and traction (c) are uncorrelated with the radial component of the density gradient (d) (Pearson's correlation coefficient R = -0.06 and 0.07, respectively). (e–h) For a confined monolayer (e), radial velocity (f) and radial traction (g) are similarly uncorrelated with the radial component of density gradient (h) (Pearson's correlation coefficient R = 0.03 and -0.12, respectively). (i–l) Histograms of the angle between the directions of density gradient and velocity (i, k) or density gradient and traction (j, l) for the expanding (i, j) or confined (k, l) islands. Each gray line shows the histogram for a single point in time for a cell island; the blue lines show histograms for all points in time. Computation of all density gradients reports data points located at least 50 μm from the boundary of the cell island so as to avoid errors in computing the density gradient near the outside of the island where density is zero.

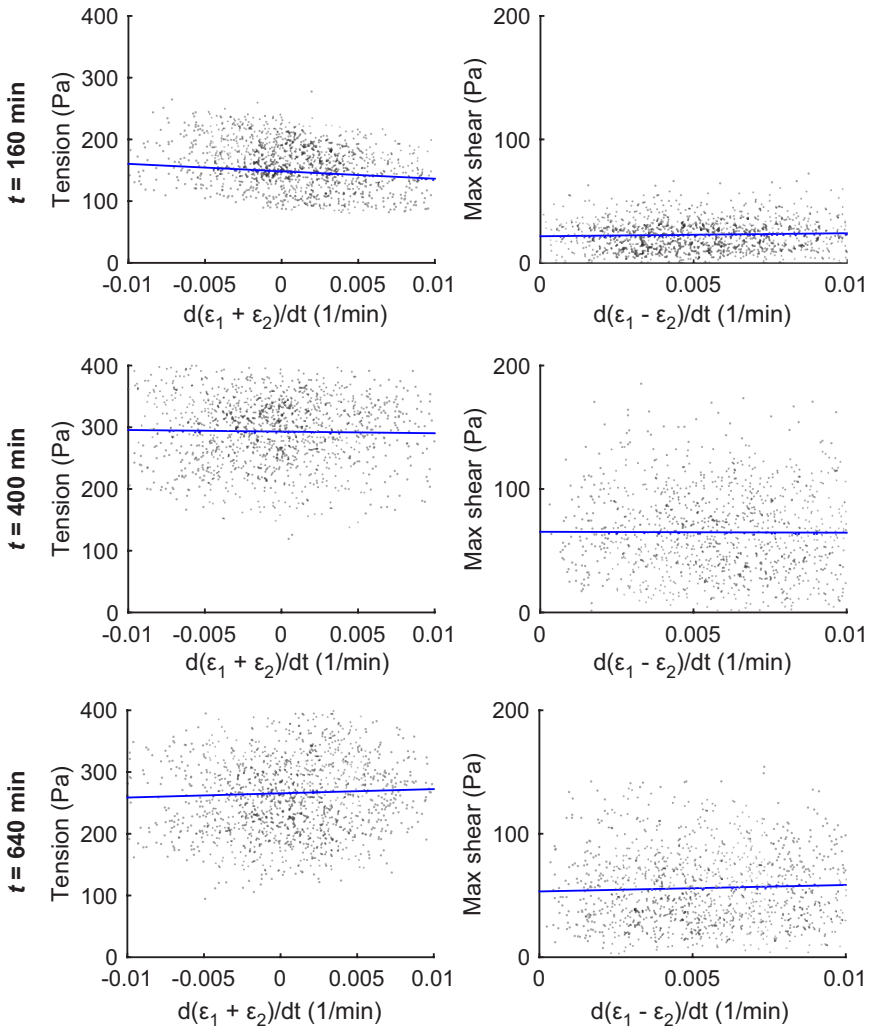

Supporting Figure S4: Negligible viscous stress in the monolayer. To investigate the role of viscosity in the monolayer, the tension (defined as the mean of the principal stresses) is compared to the sum of the principal strain rates, and the maximal shearing stress (defined as half the difference of the principal stresses) is compared to the difference of the principal strain rates. The data shown is for the cell island of Fig. 1 at time points 160, 400, and 640 min. Each dot represents a different location in the island; the blue lines show linear fits. Correlation coefficient magnitudes are typically smaller than 0.1, indicating viscosity has a negligible contribution to the stress tensor.

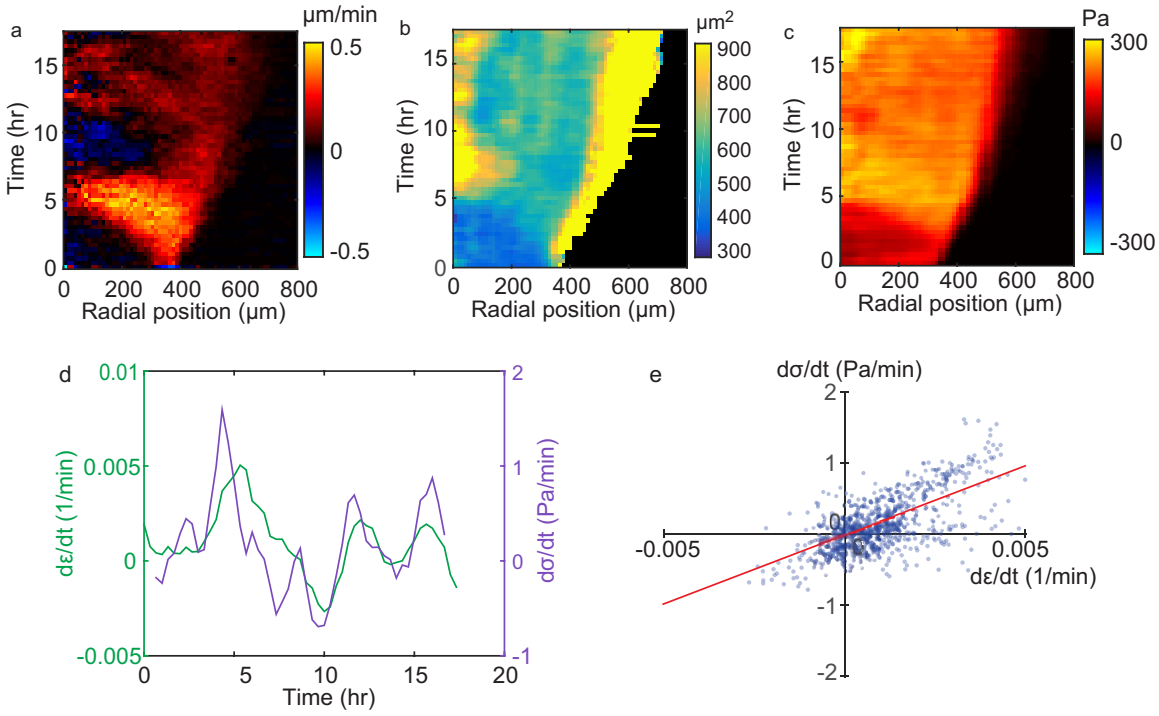

Supporting Figure S5: The elasticity of the monlayer is tested using an expanding island of MDCK cells. (a) As shown in the kymograph of radial velocity, when a circular island of cells expands outward, a wave of motion propagates from the periphery to the interior. (b) Kymograph of cell area showing area increases when each cell begins to move. (c) Kymograph of tension shows tension within each cell increases as area increases. (d) A trace of the kymographs of area strain rate $d\varepsilon/dt$ (defined as the trace of the rate-of-strain tensor) and time derivative of tension $d\sigma/dt$ along a radial position of 100 μm shows a correlation (Pearson's correlation coefficient R = 0.67). (e) A scatter plot of all points in space and time for this monolayer shows $d\sigma/dt$ is correlated with $d\varepsilon/dt$ (R = 0.64), indicating elastic behavior with a modulus K (given by the slope of a linear fit) of 71 Pa for this cell island. An average over 8 cell islands gives $K = 62 \pm 17$ Pa (mean $\pm$ standard deviation).

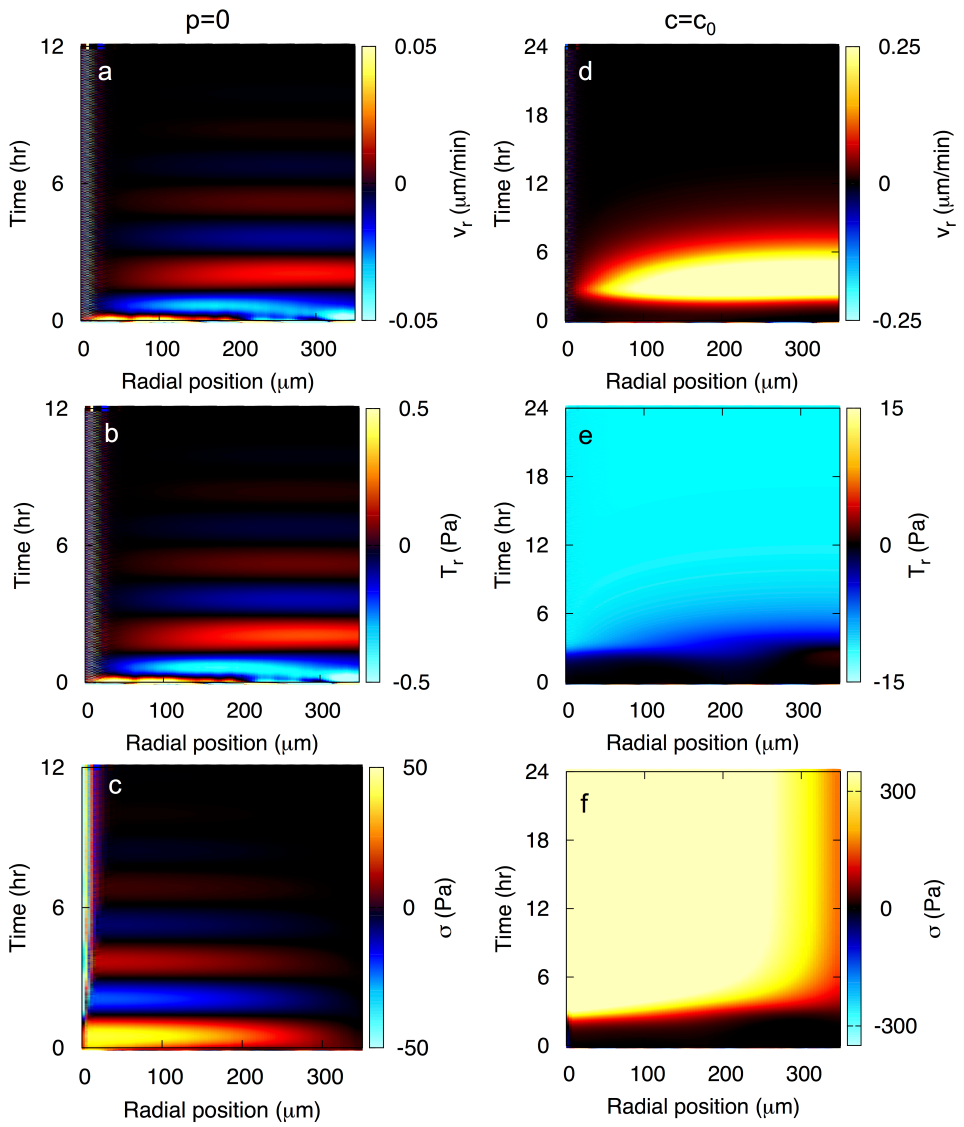

Supporting Figure S6: Limiting cases of the minimal physical model. (a–c) **u**-c model: Deformation **u** is coupled to c only. The polarization field **p** is set to zero and $\tau = 0.12$ hrs. Rest of the parameters are the same as in Supporting Table S1. In this case we obtain standing waves seen in the kymograph of velocity (a) qualitatively similar to our experiments. However, the traction (b) is proportional to velocity and is very different from the traction observed in our experiments. The monolayer tension (c) oscillated out of phase with velocity with both positive and negative values in disagreement to our experimental data. (d–f) **u**-**p** model: Deformation **u** is coupled to **p** only with the concentration field c set to its equilibrium value c_0. Simulation parameters are the same as in Supporting Table S1. In this case no wave-like behavior is obtained, indicating that the feedback between mechanical strain and the regulatory biochemistry of c is essential to explain the presence of wave-like dynamics.

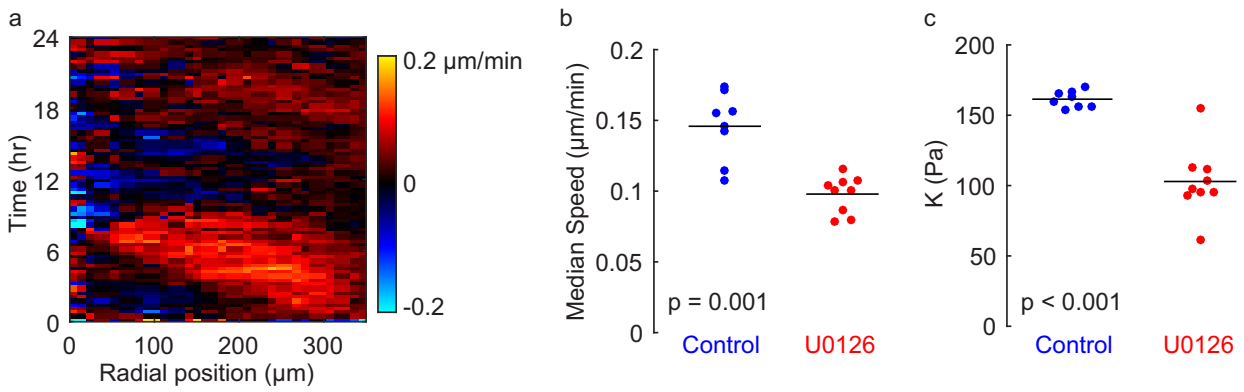

Supporting Figure S7: ERK inhibition. The ERK inhibitor U0126 (10 μM) decreases the velocity and eliminates the waves. (a) Kymograph of velocity shows no waves of cellular motion are present. (b) Compared to control, cell islands treated with U0126 move at a slower speed. (c) Compared to control, treatment with U0126 reduces the elastic modulus K. For the plots in (b) and (c), each dot corresponds to a different cell island. P values are computed using a rank sum statistical test.

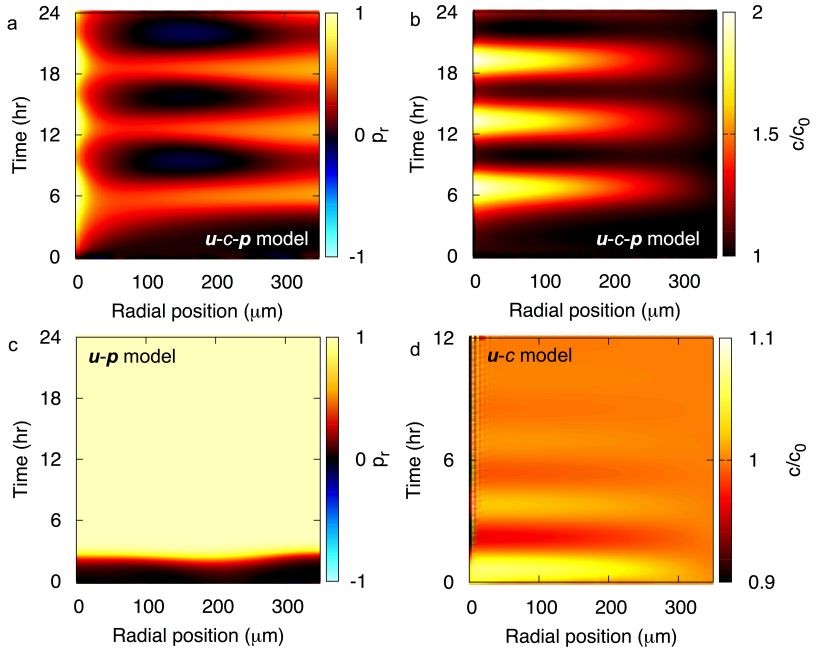

Supporting Figure S8: Dynamics of the internal state variables in the cell monolayer. (a) Kymograph of the polarization field in the full **u**-c-**p** model shows that cells at the boundary and at the center of the monolayer are polarized outwards separated by a band of inward polarized cells. (b) Kymograph of the concentration field in the full **u**-c-**p** model showing oscillations similar to the monolayer tension. (c) In the absence of coupling to c, the polarization field is uniform and points radially outward. (d) Kymograph of the concentration field in the absence of coupling to polarization field.

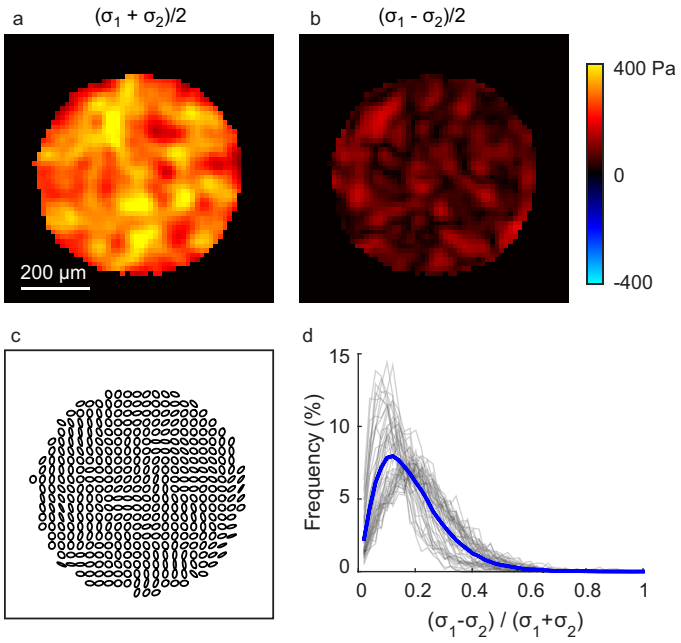

Supporting Figure S9: The stress tensor within the circular monolayers is isotropic. The first and second principal stresses, σ_1 and σ_2, are computed. (a, b) Representative plots of the mean principal stress, $(\sigma_1+\sigma_2)/2$ (a) and the maximum shear stress, $(\sigma_1-\sigma_2)/2$ (b) for a circular monolayer at one point in time. (c) Visualization of the stress tensor in the monolayer where the major and minor axes of each ellipse correspond to the magnitude of σ_1 and σ_2, and the orientation of the major axis corresponds to the orientation of the first principal stress σ_1. An ellipse that is more circular indicates a stress tensor that is more isotropic. (d) As a measure of stress isotropy, the difference in the principal stresses is divided by the sum of the principal stresses with a value of zero indicating a fully isotropic state. Histograms of $(\sigma_1-\sigma_2)/(\sigma_1+\sigma_2)$ are generated for each point in time (gray lines) and for all time points (blue line). The mean and median are <0.2, indicating the stress tensor is nearly isotropic.

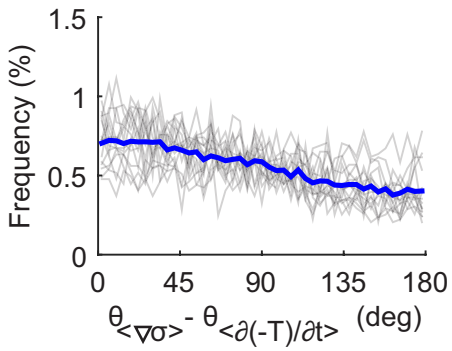

Supporting Figure S10: Cells polarize along gradients of contractility. The difference in the orientations of the gradient of tension, $\theta_{\langle\nabla\sigma\rangle}$, and the opposite of the time derivative of traction, $\theta_{\langle\partial(-\mathbf{T})/\partial t\rangle}$, is plotted as a histogram for various points in time (gray lines) and for all time points (blue line). Here, the angle brackets represent a time average over one period of oscillation. The peak near zero indicates that directions of $\langle\nabla\sigma\rangle$ and $\langle\partial(-\mathbf{T})/\partial t\rangle$ tend to align, in agreement with the model. The alignment between directions of $\langle\nabla\sigma\rangle$ and $\langle\partial(-\mathbf{T})/\partial t\rangle$ means that the cell tractions evolve in time so as to propel the cells towards regions of high tension.

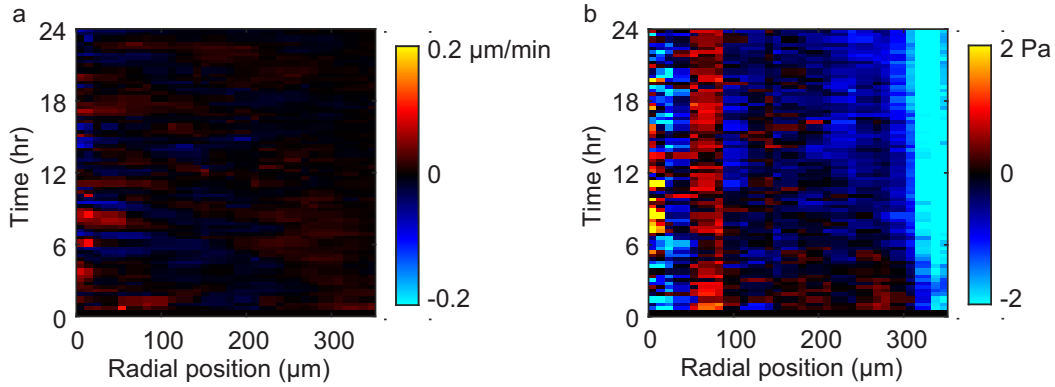

Supporting Figure S11: Blebbistatin treatment. Kymographs of (a) radial velocity and (b) radial traction for a cell island treated with blebbistatin (20 μM). The tractions are generally aligned in the opposite direction as the radial velocity. The observed anti-alignment agrees with the model when contractility is inhibited (Supporting Fig. S6 d–f). In this figure, panel (a) is the same as Fig. 4a.

Supporting Movie Legends

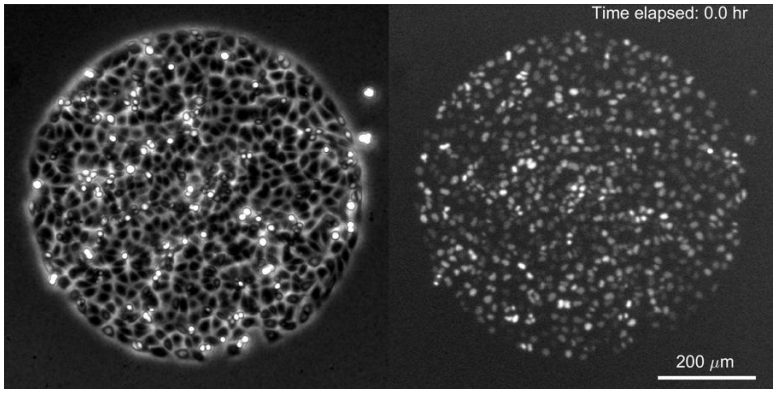

Supporting Movie 1: Oscillations of motion in a cell monolayer. Left: phase contrast; right: nuclei expressing green fluorescent protein.

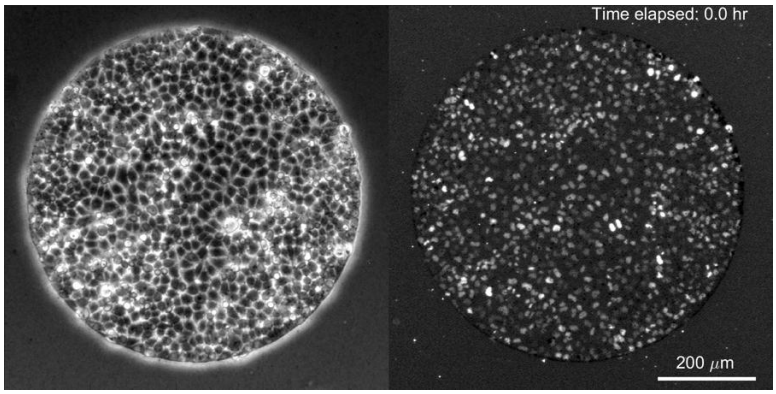

Supporting Movie 2: Motion of a cell monolayer treated with blebbistatin. Left: phase contrast; right: nuclei expressing green fluorescent protein.

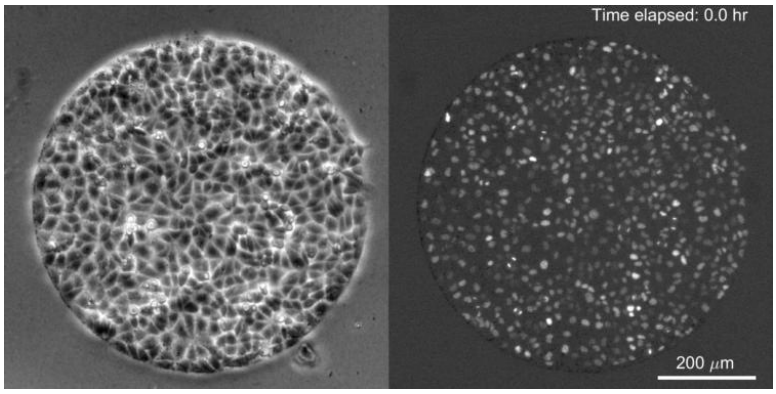

Supporting Movie 3: Motion of a cell monolayer treated with EGF. Left: phase contrast; right: nuclei expressing green fluorescent protein.

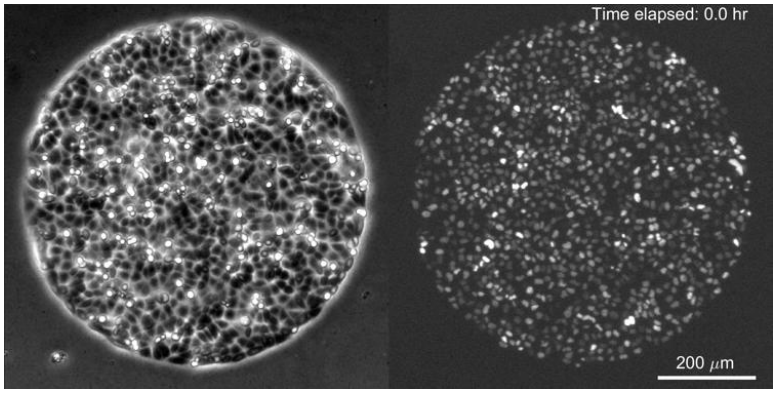

Supporting Movie 4: Motion of a cell monolayer treated with U0126. Left: phase contrast; right: nuclei expressing green fluorescent protein.